

# Crystal structure and properties of barium thorate BaThO<sub>3</sub> from first principles

Alexander I. Lebedev\*

*Physics Department, Moscow State University, Leninskie gory, 119991 Moscow, Russia*

(Dated: February 25, 2013)

The phonon spectrum of cubic BaThO<sub>3</sub> with the perovskite structure is calculated from first principles within the density functional theory. The analysis of unstable modes in the phonon spectrum enables to determine the symmetry of all possible distorted phases, calculate their energies, and show that the ground-state structure of barium thorate is *Pbnm*. For this structure, the static and optical dielectric constants, elastic moduli, heat capacity, Raman spectra, and the energy band gap in the LDA and *GW* approximations are calculated. The possibility of the structural phase transitions in BaThO<sub>3</sub> is also discussed.

PACS numbers: 61.50.Ah, 63.20.-e, 77.84.-s

## I. INTRODUCTION

The ABO<sub>3</sub> perovskite oxides constitute an important family of materials that display interesting physical properties (ferroelectricity, ferroelasticity, superconductivity, magnetism) and are widely used in technological applications. Barium thorate BaThO<sub>3</sub> is one of the members of this family. High thermal stability of barium thorate (its melting point is above 2300°C) and relatively low work function of thorium enable to use BaThO<sub>3</sub> for thermionic cathodes of high-intensity discharge lamps (see, for example, patents<sup>1-3</sup>). Barium thorate ceramics doped with neodymium<sup>4,5</sup> and yttrium<sup>6</sup> are solid electrolytes, which have the highest proton conductivity at temperatures above 900°C among solid electrolytes. Since barium thorate is produced as the fission product in nuclear reactors (especially in uranium–thorium reactors), the knowledge of its properties is also important for predicting the reliability of nuclear fuel elements.

Insufficient knowledge of the properties of BaThO<sub>3</sub> becomes evident from the fact that even its crystal structure is not well established. In the very first work,<sup>7</sup> the structure of barium thorate was identified as a simple perovskite structure with the lattice parameter of  $a \approx 4.48$  Å. A more detailed study<sup>8</sup> found the superstructure reflections on the diffraction patterns, but because of the lack of splitting of the strong peaks, the structure was considered as a pseudocubic one with a doubled lattice parameter. Finally, after the splitting of the main reflections was observed,<sup>9,10</sup> the structure of BaThO<sub>3</sub> was identified as orthorhombic, but neither the space group nor the atomic coordinates were determined.

Thermodynamic properties of barium thorate (the Gibbs energy of formation) were determined in Refs. 11 and 12. In Ref. 13, the electronic structure, optical and elastic properties of BaThO<sub>3</sub> were calculated from first principles using the FP-LAPW approach, but for some reason the calculations were limited to the cubic five-atom unit cell, whereas X-ray studies clearly indicate the lower symmetry. According to these calculations, the cubic barium thorate is a direct-gap insulator with the band gap of  $E_g = 5.7$  eV. This result, however, contradicts the density-of-states calculations presented in Ref. 13,

according to which the energy gap between the valence and conduction bands is 3.33 eV, and the calculations of the  $\epsilon_2(\omega)$  optical spectra in which the absorption starts at an energy below 5 eV.

The knowledge of the true crystal structure of BaThO<sub>3</sub> is crucial for correct prediction of its properties. In this work, we use the first-principles calculations to determine the equilibrium structure of barium thorate, calculate some of its properties, and discuss the possibility of the structural phase transitions in it.

## II. CALCULATION DETAILS

To predict the properties of BaThO<sub>3</sub>, we must first determine its ground-state structure which has the lowest energy at  $T = 0$ . For this purpose, we must first calculate the phonon spectrum of its parent *Pm3m* phase and then, by adding the distortions corresponding to unstable modes in the phonon spectrum to the structure, seek for a minimum-energy structure in which the energy of all optical phonons at all points of the Brillouin zone are positive and the structure is mechanically stable (the stability criterion is the positive values of the determinant and all leading principal minors of the 6×6 matrix of elastic moduli in the Voigt notation).<sup>14</sup>

In this work, the first-principles calculations were performed within the density functional theory (DFT) using the ABINIT software.<sup>15</sup> The exchange-correlation interaction was described in the local density approximation (LDA). Pseudopotentials for Ba and O atoms used in the calculations were taken from Ref. 14. Scalar-relativistic pseudopotential for the Th atom was constructed using the RRKJ scheme<sup>16</sup> with the OPIUM program.<sup>17</sup> To improve the transferability of the pseudopotential, the *s* local potential correction<sup>18</sup> was used. The parameters used for the construction of pseudopotentials are presented in Table I. Testing of the Th pseudopotential using ThO<sub>2</sub> as an example revealed its high enough quality: the calculated lattice parameter of this compound (5.606 Å) differed from the experimental value by only 0.15% and the bulk modulus (205 GPa) differed by 4%.

The lattice parameters and the equilibrium atomic co-

TABLE I. Electronic configuration of atoms and parameters used for construction of pseudopotentials:  $r_s$ ,  $r_p$ , and  $r_d$  are radii of the pseudopotential cores for  $s$ -,  $p$ -, and  $d$ -projections;  $q_s$ ,  $q_p$ , and  $q_d$  are the cut-off wave vectors used in the optimization procedure;  $r_{\min}$ ,  $r_{\max}$ , and  $V_{\text{loc}}$  are the range limits and depth of the correcting local potential. All the values are in Hartree atomic units except for the correction energy which is in Ry.

Atom	Configuration	$r_s$	$r_p$	$r_d$	$q_s$	$q_p$	$q_d$	$r_{\min}$	$r_{\max}$	$V_{\text{loc}}$
Ba	$5s^2 5p^6 5d^0 6s^0$	1.85	1.78	1.83	7.07	7.07	7.07	0.1	1.68	1.95
Th	$6s^2 6p^6 6d^0 7s^0$	1.88	2.04	2.04	7.57	7.27	7.07	0.01	1.76	0.75
O	$2s^2 2p^4 3d^0$	1.40	1.55	1.40	7.07	7.57	7.07	—	—	—

ordinates in the unit cell were determined from the condition that the residual forces acting on the atoms are less than  $5 \cdot 10^{-6}$  Ha/Bohr (0.25 meV/Å) and the total energy is calculated self-consistently to an accuracy of better than  $10^{-10}$  Ha. The integration over the Brillouin zone was performed on the  $8 \times 8 \times 8$  Monkhorst–Pack mesh for the cubic phase or on the meshes with equivalent  $k$ -point density for low-symmetry phases. The maximum plane-wave energy was 30 Ha.

The quasiparticle band gap of BaThO<sub>3</sub> was calculated using the so-called one-shot  $GW$  approximation.<sup>19,20</sup> The Kohn–Sham wave functions and energies calculated within DFT-LDA were used as a zeroth-order approximation. The dielectric matrix  $\epsilon_{\mathbf{G}\mathbf{G}'}(\mathbf{q}, \omega)$  was computed for a  $6 \times 6 \times 6$   $\mathbf{q}$ -point mesh from the independent-particle polarizability matrix  $P_{\mathbf{G}\mathbf{G}'}^0(\mathbf{q}, \omega)$  calculated for 3743 reciprocal-lattice vectors  $\mathbf{G}(\mathbf{G}')$ , 20 occupied and 280 unoccupied bands. The dynamic screening was described using the Godby–Needs plasmon-pole model. The components of wave functions with kinetic energy up to 24 Ha were used in these calculations. The energy correction to the DFT-LDA solution was computed as diagonal matrix elements of the  $[\Sigma - E_{xc}]$  operator, where  $\Sigma = GW$  is the self-energy operator,  $E_{xc}$  is the exchange-correlation energy operator,  $G$  is the Green’s function, and  $W = \epsilon^{-1}v$  is the screened Coulomb interaction. In the calculations of  $\Sigma$ , the components of wave functions with kinetic energy up to 24 Ha for both exchange and correlation parts of  $\Sigma$  were used. The accuracy of the band gap calculation estimated from the convergence tests is  $\sim 0.05$  eV.

### III. RESULTS

The phonon spectrum of BaThO<sub>3</sub> in the cubic  $Pm3m$  phase is shown in Fig. 1. It is seen that there are nine unstable modes in the phonon spectrum of barium thorate. They include the triply degenerate  $\Gamma_{15}$  mode associated with the ferroelectric instability; the triply degenerate  $\Gamma_{25}$  mode describing the uniform deformation of the oxygen octahedra; the triply degenerate  $R_{25}$  mode and nondegenerate  $M_3$  mode, which describe the rotation of the octahedra; the doubly degenerate antiferroelectric  $X_5$ ,  $X'_5$ , and  $M'_5$  modes; the non-degenerate  $X_3$  mode describing spatially non-uniform deformation of the oc-

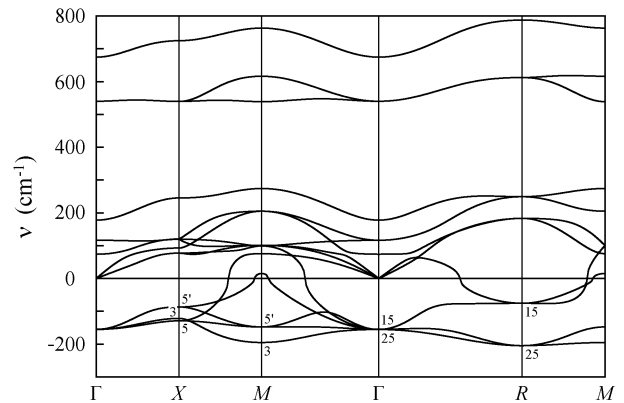


FIG. 1. Phonon spectrum of BaThO<sub>3</sub> in the cubic  $Pm3m$  phase. The labels indicate the symmetry of unstable modes.

tahedra; and the triply degenerate  $R_{15}$  mode describing the vibrations of the Ba atom in its oxygen environment.

The energies of all phases obtained from the condensation of the unstable phonons as well as the energies of  $Pbnm$  and  $Cmcm$  phases resulting from simultaneous condensation of the  $R_{25}$  and  $M_3$  modes are given in Table II. Among these phases, the  $Pbnm$  phase has the lowest energy.

The calculation of the phonon spectrum in the  $Pbnm$  phase shows that the frequencies of all optical phonons at the center of the Brillouin zone and at the high-symmetry points on its boundary are positive; the determinant and all leading principal minors constructed from the elastic tensor are also positive. This means that the  $Pbnm$  phase is the ground-state structure of BaThO<sub>3</sub>. The calculated lattice parameters of this phase are  $a = 6.3140$ ,  $b = 6.4039$ , and  $c = 8.9578$  Å; the atomic coordinates are given in Table III. The obtained lattice parameters are in good agreement with the experimental data of Ref. 9 ( $a = 6.345 \pm 0.002$ ,  $b = 6.376 \pm 0.002$ ,  $c = 8.992 \pm 0.002$  Å) and Ref. 10 ( $a = 6.35 \pm 0.01$ ,  $b = 6.387 \pm 0.009$ ,  $c = 8.995 \pm 0.009$  Å).

We now consider some physical properties of BaThO<sub>3</sub> in the ground state. Although the ferroelectric instability was found in the parent cubic phase, the structural distortions suppress this instability, and in the ground state barium thorate is a paraelectric. The static di-

TABLE II. The relative energies of the low-symmetry phases of BaThO<sub>3</sub> resulting from the condensation of unstable modes. The most stable phase is in boldface.

Phase	Unstable mode	Energy (meV)
<i>Pm3m</i>	—	0
<i>P4<sub>2</sub>/mmc</i>	$X_3$	-55.9
<i>Cmcm</i>	$X'_5$	-90.9
<i>Pmma</i>	$X_5$	-99.3
<i>Pmma</i>	$X'_5$	-101.4
<i>Cmcm</i>	$X_5$	-118.8
<i>I4/mmm</i>	$R_{15}$	-123.0
<i>R3m</i>	$R_{15}$	-148.0
<i>P4m2</i>	$\Gamma_{25}$	-153.1
<i>Amm2</i>	$\Gamma_{15}; \Gamma_{25}$	-228.0
<i>Pmma</i>	$M'_5$	-234.5
<i>R32</i>	$\Gamma_{25}$	-255.9
<i>Cmmm</i>	$M'_5$	-303.2
<i>R3m</i>	$\Gamma_{15}$	-326.4
<i>P4mm</i>	$\Gamma_{15}$	-337.2
<i>P4/mbm</i>	$M_3$	-529.2
<i>I4/mcm</i>	$R_{25}$	-599.3
<i>Cmcm</i>	$R_{25} + M_3$	-696.4
<i>R3c</i>	$R_{25}$	-710.1
<i>Imma</i>	$R_{25}; R_{15}$	-754.4
<b><i>Pbnm</i></b>	<b><math>R_{25} + M_3</math></b>	<b>-797.8</b>

TABLE III. Calculated atomic coordinates in the orthorhombic *Pbnm* phase of barium thorate.

Atom	Position	$x$	$y$	$z$
Ba	4c	-0.01246	0.03717	0.25000
Th	4b	0.50000	0.00000	0.00000
O1	4c	0.10447	0.46199	0.25000
O2	4d	0.70713	0.29227	0.05723

electric tensor in the *Pbnm* phase is characterized by three diagonal components of  $\epsilon_{xx}^0 = 24.7$ ,  $\epsilon_{yy}^0 = 25.0$ , and  $\epsilon_{zz}^0 = 37.6$ ; the tensor of the optical dielectric constant is described by the components of  $\epsilon_{xx}^\infty = 4.42$ ,  $\epsilon_{yy}^\infty = 4.35$ , and  $\epsilon_{zz}^\infty = 4.28$ . The elastic moduli are  $C_{11} = 195$  GPa,  $C_{22} = 200$  GPa,  $C_{33} = 199$  GPa,  $C_{12} = 99$  GPa,  $C_{13} = 83$  GPa,  $C_{23} = 71$  GPa,  $C_{44} = 55$  GPa,  $C_{55} = 51$  GPa,  $C_{66} = 64$  GPa. The bulk modulus in the orthorhombic phase is  $B = 121.9$  GPa; in the *Pm3m* phase its value is 124.2 GPa and is very close to the value of 124 GPa obtained in Ref. 13.

For identification of the *Pbnm* phase of BaThO<sub>3</sub> it is convenient to use the Raman spectroscopy. The calculated frequencies of the Raman-active modes in this phase are given in Table IV, and the theoretical Raman spectrum calculated for a polycrystalline sample at 300 K using the formulas from Ref. 21 is shown in Fig. 2.

TABLE IV. Calculated frequencies of the Raman-active modes for the *Pbnm* phase of barium thorate.

The mode symmetry	Frequency (cm <sup>-1</sup> )
$A_g$	75; 89; 157; 207; 300; 341; 523
$B_{1g}$	95; 109; 169; 283; 312; 387; 666
$B_{2g}$	92; 217; 331; 508; 681
$B_{3g}$	96; 123; 298; 520; 613

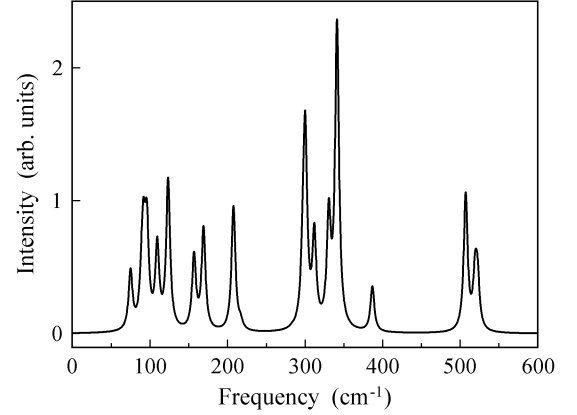


FIG. 2. Calculated Raman spectra for a polycrystalline sample of BaThO<sub>3</sub> at 300 K.

The energies of different phases obtained in this work (Table II) enable to make some remarks on the possible phase transitions in barium thorate. The *Imma* phase closest in energy to the *Pbnm* ground-state structure has the energy only by 43.4 meV higher than the ground-state energy. This means that a second-order phase transition *Pbnm*  $\rightarrow$  *Imma* can occur in BaThO<sub>3</sub> at a temperature

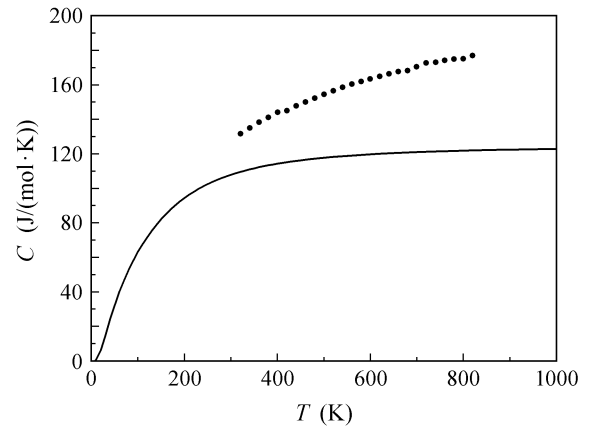


FIG. 3. Comparison of the calculated heat capacity  $C_v$  in the *Pbnm* phase of barium thorate (solid line) with the experimental data<sup>22</sup> (points).

slightly above 300 K. In the experimental study of the heat capacity,<sup>22</sup> no anomalies were detected in the temperature range 320–820 K, but the peculiarity of the results of Ref. 22 is that the measured values of the specific heat are much higher than our calculated ones (Fig. 3) and, more significantly, they even exceed the theoretical limit of  $3R$  per atom in the unit cell (the Dulong–Petit law). This may indicate that the investigated sample was likely not pure.<sup>23</sup> We believe that the predicted phase transition was hidden by this fact. In this regard, we note that the features in the dielectric properties of BaThO<sub>3</sub> at about 260°C, which were observed in Ref. 24 and interpreted as an evidence for the ferroelectric phase transition, can actually be associated with the  $Pbnm \rightarrow Imma$  phase transition under discussion.

To resolve the contradictions mentioned in the Introduction on the energy band gap  $E_g$  in cubic BaThO<sub>3</sub>, we performed our own calculations of  $E_g$  in both the LDA approximation used in this work and in the  $GW$  approximation<sup>19,20</sup> which takes into account the many-body effects and enables to obtain the energy band gap in much better agreement with the experiment.<sup>25</sup> According to our data, in the LDA approximation  $E_g^{\text{LDA}} = 2.907$  eV in the  $Pm3m$  phase; in the orthorhombic  $Pbnm$  phase

the band gap increases to 3.947 eV. As the DFT calculations always underestimate the energy band gap, more realistic  $E_g$  values can be obtained in the  $GW$  approximation. These calculations gave the energy band gap  $E_g^{\text{GW}} \approx 4.40$  eV for the cubic phase. This value is intermediate between the two values, 5.7 eV and 3.33 eV, reported for this phase in Ref. 13. In both cubic and orthorhombic phases, the extrema of the valence and conduction bands are located at the  $\Gamma$  point of the Brillouin zone (the optical transitions are direct).

The calculations presented in this work were performed on the laboratory computer cluster (16 cores).

#### IV. CONCLUSIONS

First-principles calculations of the phonon spectra and structure of cubic BaThO<sub>3</sub> and its distorted phases have shown that the ground-state structure of barium thorate is  $Pbnm$ . The static and optical dielectric constants, elastic moduli, heat capacity, Raman spectra, and the energy band gap in the LDA and  $GW$  approximations have been calculated for this structure. It has been shown that the structural phase transition  $Pbnm \rightarrow Imma$  can occur in BaThO<sub>3</sub> at a temperature slightly above 300 K.

---

\* swan@scon155.phys.msu.ru

<sup>1</sup> S. H. Noble and H. P. Rooksby, “Activated electrode,” U.S. Patent No. 2,394,095 (05 Feb 1946).

<sup>2</sup> J. E. White, “Thermoionic electrode for discharge lamps,” U.S. Patent No. 3,029,359 (10 Apr 1962).

<sup>3</sup> D. M. Speros, “Cathodes and method of manufacture,” U.S. Patent No. 3,188,236 (08 June 1965).

<sup>4</sup> T. Tsuji, T. Suzuki, and H. Iwahara, *Solid State Ionics* **70–71**, 291 (1994).

<sup>5</sup> K. A. Furøy, R. Haugsrud, M. Hänsel, A. Magrasó, and T. Norby, *Solid State Ionics* **178**, 461 (2007).

<sup>6</sup> T. Tsuji, N. Miyajima, and M. Ochida, *Solid State Ionics* **79**, 183 (1995).

<sup>7</sup> A. Hoffmann, *Z. Physik. Chem. B* **28**, 65 (1935).

<sup>8</sup> A. J. Smith and A. J. E. Welch, *Acta Cryst.* **13**, 653 (1960).

<sup>9</sup> T. Nakamura, *Chem. Lett.* **3**, 429 (1974).

<sup>10</sup> R. D. Purohit, A. K. Tyagi, M. D. Mathews, and S. Saha, *J. Nucl. Mater.* **280**, 51 (2000).

<sup>11</sup> S. R. Bharadwaj, R. Mishra, M. Ali(Basu), D. Das, A. S. Kerkar, and S. R. Dharwadkar, *J. Nucl. Mater.* **275**, 201 (1999).

<sup>12</sup> R. Mishra, M. Ali(Basu), S. R. Bharadwaj, A. S. Kerkar, D. Das, and S. R. Dharwadkar, *J. Alloys Comp.* **290**, 97 (1999).

<sup>13</sup> G. Murtaza, I. Ahmad, B. Amin, A. Afaq, M. Maqbool, J. Maqssod, I. Khan, and M. Zahid, *Opt. Mater.* **33**, 553 (2011).

<sup>14</sup> A. I. Lebedev, *Phys. Solid State* **51**, 362 (2009).

<sup>15</sup> X. Gonze, B. Amadon, P.-M. Anglade, J.-M. Beuken, F. Bottin, P. Boulanger, F. Bruneval, D. Caliste, R. Caracas, M. Côté, T. Deutsch, L. Genovese, P. Ghosez, M. Gi-

antomassi, S. Goedecker, D. R. Hamann, P. Hermet, F. Jollet, G. Jomard, S. Leroux, M. Mancini, S. Mazevet, M. J. T. Oliveira, G. Onida, Y. Pouillon, T. Rangel, G.-M. Rignanese, D. Sangalli, R. Shaltaf, M. Torrent, M. J. Verstraete, G. Zerah, and J. W. Zwanziger, *Computer Phys. Commun.* **180**, 2582 (2009).

<sup>16</sup> A. M. Rappe, K. M. Rabe, E. Kaxiras, and J. D. Joannopoulos, *Phys. Rev. B* **41**, 1227 (1990).

<sup>17</sup> “Opium—pseudopotential generation project,” <http://opium.sourceforge.net>

<sup>18</sup> N. J. Ramer and A. M. Rappe, *Phys. Rev. B* **59**, 12471 (1999).

<sup>19</sup> G. Onida, L. Reining, and A. Rubio, *Rev. Mod. Phys.* **74**, 601 (2002).

<sup>20</sup> F. Bechstedt, F. Fuchs, and G. Kresse, *Phys. Status Solidi B* **246**, 1877 (2009).

<sup>21</sup> S. A. Prosandeev, U. Waghmare, I. Levin, and J. Maslar, *Phys. Rev. B* **71**, 214307 (2005).

<sup>22</sup> R. V. Krishnan, K. Nagarayan, and P. R. V. Rao, *J. Nucl. Mater.* **299**, 28 (2001).

<sup>23</sup> It is known that, when exposed to air, barium thorate absorbs moisture and reacts with CO<sub>2</sub> thus forming a mixture of ThO<sub>2</sub> + BaCO<sub>3</sub>.<sup>7,24</sup> The annealing temperature before the specific heat measurements in Ref. 22 (550°C) was sufficient to remove moisture, but was not high enough to decompose BaCO<sub>3</sub>. After the interaction with CO<sub>2</sub>, the number of atoms in a mole of the substance increases, and this results in an increase of the heat capacity.

<sup>24</sup> Y. Harada and S. W. Bradstreet, *Synthesis of refractory mixed oxide with perovskite structure*, Tech. Rep. ARF-6046 (Illinois Inst. of Technol., Chicago. Armour Research Foundation, 1960).

<sup>25</sup> A. I. Lebedev, *Phys. Solid State* **54**, 1663 (2012).